Abstracta

Ano XIII - N. 05

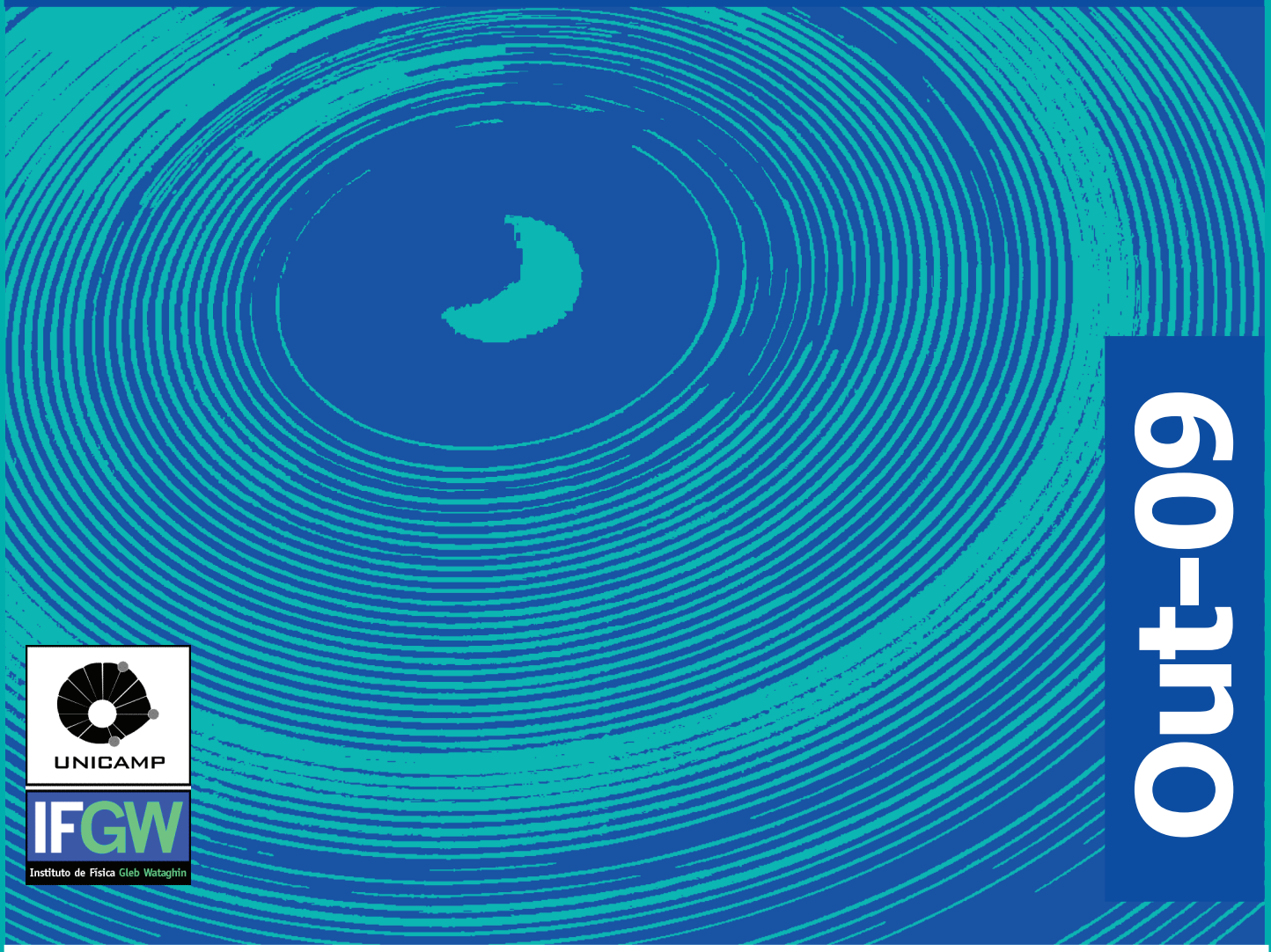

Out-09

UNICAMP

IFGW

Instituto de Física Gleb Wataghin

Trabalhos Publicados

Setembro 2009 à Outubro 2009

P169-09 à P203 -09

Trabalhos Publicados

P169-09 "A modified time-dependent perturbation approach to quantum dynamics and its application to relaxation phenomena in magnetic molecules"

Dartora, C. A., Cabrera, G. G., and Nobrega, K. Z.

We introduce a modified version of the interaction picture applicable to situations in which the nonperturbed Hamiltonian is time-dependent but can be diagonalized by the same basis of states at all times. We probe the method using a simple model Hamiltonian to study the spin dynamics of molecular magnets with time-dependent fields. Fully quantum mechanical calculations show the superiority. of our method compared to the usual time-dependent perturbation theory. Our approach takes into account time-dependent fields and converges rapidly to the exact solution. (C) 2009 American Association of Physics Teachers. [DOI: 10.1119/1.3133088]

American Journal of Physics 77[8], 742-745. 2009.

P170-09 "A Multitechnique Study of Structure and Dynamics of Polyfluorene Cast Films and the Influence on Their Photoluminescence"

Faria, G. C., Plivelic, T. S., Cossiello, R. F., Souza, A. A., Atvars, T. D. Z., Torriani, I. L., and deAzevedo, E. R.

This article describes the microstructure and dynamics in the solid state of polyfluorene-based polymers, poly(9,)-dioctylfluorenyl-2,7-diyl) (PFO), a semicrystalline polymer, and poly [(9,9-dioctyl- 2,7-divinylene-fluorenylene)-alt-co-{2-methoxy-5-(2-ethyl-hexyloxy)- 1,4-phenylene vinylene}, a copolymer with mesomorphic phase properties. These Structures were determined by wide-angle X-ray scattering (WAXS) measurements, Assuming a packing model for the copolymer structure, where the planes of the phenyl rings are stacked and separated by an average distance of similar to 4.5 angstrom and laterally spaced by about similar to 16 angstrom, we followed the evolution of these distances as a function of temperature using WAXS and associated the changes observed to the polymer relaxation processes identified by dynamical mechanical thermal analysis. Specific molecular motions were studied by solid-state nuclear magnetic resonance. The onset of the side-chain motion at about 213 K (beta-relaxation) produced a small increase in the lateral spacing and in the stacking distance of the phenyl rings in them aggregated Structures, Besides, at about 383 K (alpha-relaxation) there occurs a significant increase in the amplitude of the torsion motion in the backbone, producing a greater increase in the stacking distance of the phenyl rings. Similar results were observed in the semicrystalline phase of PFO, but in this case the presence of the crystalline structure affects considerably the overall dynamics, which tends to be more hindered. Put together, Our data explain many features of the temperature dependence of the photoluminescence of these two polymers

Journal of Physical Chemistry B 113[33], 11403-11413. 2009.

P171-09 "C-60-derived nanobaskets: stability, vibrational signatures, and molecular trapping"

dos Santos, S. G., Pires, M. S., Lemos, V., Freire, V. N., Caetano, E. W. S., Galvao, D. S., Sato, F., and Albuquerque, E. L.

C-60-derived nanobaskets, with chemical formulae (symmetry point group) C40H10 (C-5v), C39H12 (C-3v), C46H12 (C-2v), were investigated. Molecular dynamic simulations (MDSs) indicate that the molecules preserve their bonding frame for temperatures up to 300 K (simulation time 100 ps), and maintain atomic cohesion for at least 4 ps at temperatures up to 3500 K. The infrared spectra of the C-60-derived nanobaskets were simulated through density functional theory (DFT) calculations, allowing for the attribution of infrared signatures specific to each carbon nanobasket. The possibility of using C-60-derived nanobaskets as molecular containers is demonstrated by performing a DFT study of their bonding to hydrogen, water, and L-alanine. The carbon nanostructures presented here show a higher bonding energy (similar to 1.0 eV), suggesting that a family of nanostructures, C-n-derived (n = 60, 70, 76, 80, etc) nanobaskets, could work as molecular containers, paving the way for future developments such as tunable traps for complex molecular systems

Nanotechnology 20[39], 395701. 2009.

P172-09 "Coexisting on-center and off-center Yb3+ sites in Ce1-xYbxFe4P12 skutterudites"

Garcia, F. A., Garcia, D. J., Avila, M. A., Vargas, J. M., Pagliuso, P. G., Rettori, C., Passeggi, M. C. G., Oseroff, S. B., Schlottmann, P., Alascio, B., and Fisk, Z.

Electron-spin-resonance (ESR) measurements performed on the filled skutterudite system Ce1-xYbxFe4P12 (x less than or similar to 0.003) unequivocally reveal the coexistence of two Yb3+ resonances associated with sites of considerably different occupations and temperature behaviors. Detailed analysis of the ESR data suggests a scenario where the fraction of oversized (Fe2P3)(4) cages that host Yb ions are filled with a low occupation of on-center Yb3+ sites and a highly occupied T-dependent distribution of off-center Yb3+ sites. Analysis of the Yb-171(3+)(I=1/2) isotope hyperfine splittings reveal that these two sites are associated with a low (similar to 1 GHz) and a high (greater than or similar to 15 GHz) rattling frequency, respectively. Our findings introduce Yb3+ in T-h symmetry systems and use the Yb3+ ESR as a sensitive microscopic probe to investigate the Yb3+ ions dynamics

Physical Review B 80[5], 052401. 2009.

P173-09 "Computerized texture analysis of histologic sections: comparison of aortas of normotensive and hypertensive patients"

Metze, K., Vieira, G., Adam, R. L., Ferro, D. P., de Thomaz, A. A., and Cesar, C. L.

Virchows Archiv 455, 81-82. 2009.

P174-09 "Defect-mediated half-metal behavior in zigzag graphene nanoribbons"

Oeiras, R. Y., raujo-Moreira, F. M., and da Silva, E. Z.

In this work, we present ab initio studies of the electronic and transport properties of carbon nanoribbons with structural defects: divacancies and divacancies combined with the Stone-Wales-like (SW) defects. Simulations with defects in different positions with respect to the ribbons indicated that the total energy of the ribbon is lower when the defect is at the ribbon edge. This indicates that the

energy of the ribbon is lower when the defect is at the ribbon edge. This indicates that the relation defect edge is of fundamental importance to find the minimal energy configuration. All ribbons studied in this Brief Report show a high spin polarization in the transmittance, in some cases more than 90%, showing an almost half metal behavior suggesting them as possible candidates to be used as spin filter systems

Physical Review B 80[7], 073405. 2009.

P175-09 "Ferromagnetic Properties of Bulk Fe-doped CeO2 Dilute Magnetic Semiconductors"

Sharma, S. K., Knobel, M., Meneses, C. T., Kumar, S., Kim, Y. J., Koo, B. H., Lee, C. G., Shukla, D. K., and Kumar, R.

Polycrystalline Fe-doped Ce1-xFexO2-delta has been fabricated by using the standard solid state reaction technique in the concentration range 0 <= x <= 0.05. Reitveld refinement of the X-ray diffraction patterns shows a pure CeO2 phase when x <= 0.03, and the appearance of a secondary impurity phase of Fe2O3 beyond that. Furthermore, by doping Fe into CeO2 powder, the ferromagnetism can be significantly enhanced to a maximum value for x = 0.03, but degrades quickly with further doping. Magnetization results reveal that the large room-temperature ferromagnetism observed in Fe-doped CeO2 powder originates from a combined effect of oxygen vacancies and transition metal doping

Journal of the Korean Physical Society 55[3], 1018-1021. 2009.

P176-09 "Ferromagnetism in Chemically-synthesized Co-doped ZnO"

Kumar, S., Kim, Y. J., Koo, B. H., Choi, H., Lee, C. G., Sharma, S. K., Knobel, M., Gautam, S., and Chae, K. H.

We report; room temperature ferromagnetism (RTFM) in Co-doped ZnO (Zn1-xCoxO; x = 0.01 - 0.05) powder synthesized using a co-precipitation method. Our magnetometry data reveal a weak FM behavior at RT in the range 0.01 < x < 0.05. FM by magnetic FM moment steadily decreases with increasing dopant. The O K-edge near-edge X-ray absorption fin e structure (NEXAFS) spectra indicate that 0 vacancies increases with increasing Co concentration and that the sample with X >= 0.03 has more broadening at 535 and 540 eV, which may be due to the oxygen vacancies. Co in the ZnO host reveals a +2 oxidation state via the K edge NEXAFS spectra

Journal of the Korean Physical Society 55[3], 1060-1064. 2009.

P177-09 "First-principles prediction of a metastable crystalline phase of Ga with Cmcm symmetry"

de Koning, M., Antonelli, A., and Jara, D. A. C.

We report on evidence for the existence of an unknown metastable crystalline phase of gallium by the combination of classical molecular-dynamics (MD) simulations and density-functional theory (DFT) calculations. The MD simulations, based on a modified embedded-atom potential, reveal the unknown crystalline form through a first-order phase transition originating from the Cmca symmetric alpha-Ga phase under hydrostatic tension. Subsequently, the DFT calculations using two different generalized-gradient approximation functionals are employed to verify its stability and determine its electronic structure. The structure of the orthorhombic phase is described by symmetry group Cmcm and shows a dimer arrangement resembling the alpha-Ga phase. A first-order phase transition from alpha-Ga to the unknown phase is estimated to occur at -1.3 GPa

Physical Review B 80[4], 045209. 2009.

P178-09 "Fractal analysis of Xylella fastidiosa biofilm formation"

Moreau, A. L. D., Lorite, G. S., Rodrigues, C. M., Souza, A. A., and Cotta, M. A.

We have investigated the growth process of Xylella fastidiosa biofilms inoculated on a glass. The size and the distance between biofilms were analyzed by optical images; a fractal analysis was carried out using scaling concepts and atomic force microscopy images. We observed that different biofilms show similar fractal characteristics, although morphological variations can be identified for different biofilm stages. Two types of structural patterns are suggested from the observed fractal dimensions D-f. In the initial and final stages of biofilm formation, D-f is 2.73 + 0.06 and 2.68 + 0.06, respectively, while in the maturation stage, D-f = 2.57 + 0.08. These values suggest that the biofilm growth can be understood as an Eden model in the former case, while diffusion-limited aggregation (DLA) seems to dominate the maturation stage. Changes in the correlation length parallel to the surface were also observed; these results were correlated with the biofilm matrix formation, which can hinder nutrient diffusion and thus create conditions to drive DLA growth. (C) 2009 American Institute of Physics. [DOI: 10.1063/1.3173172]

Journal of Applied Physics 106[2], 024702. 2009.

P179-09 "Generalized purity and quantum phase transition for Bose-Einstein condensates in a symmetric double well"

Viscondi, T. F., Furuya, K., and de Oliveira, M. C.

The generalized purity is employed for investigating the process of coherence loss and delocalization of the Q function in the Bloch sphere of a two-mode Bose-Einstein condensate in a symmetrical double well with cross collision. Quantum phase transition of the model is signaled by the generalized purity as a function of an appropriate parameter of the Hamiltonian and the number of particles (N). A power-law dependence of the critical parameter with N is derived

Physical Review A 80[1], 013610. 2009.

P180-09 "Imaging by means of a simple diffractive or refractive element: the axicon"

Lunazzi, J. J. and Magalhaes, D. S. F.

In this previously divulgated paper [1] we demonstrate that the light diffracted by a simple compact disc call be used to generate images with interesting basic attributes. We compare this attributes with the ones obtained with refractive elements. A compact disc acts as an axicon that generates a diffraction-free beam and, because the focused position of the image depends oil the wavelength of the diffracted light, thus it can be useful as a spectral filter. The experiments are of easy reproduction, allowing the understanding of images that the students observe daily at school or at home

Revista Brasileira de Ensino de Fisica 31[2], 2501. 2009.

P181-09 "Influence of air-filling fraction on forward Raman-like scattering by transversely trapped acoustic resonances in photonic crystal fibers"

Brenn, A., Wiederhecker, G. S., Kang, M. S., Hundertmark, H., Joly, N., and Russell, P. S.

Raman-like forward scattering by acoustic phonons transversely trapped in birefringent silica-air photonic crystal fibers is studied. As the air-filling fraction increases, core-confined acoustic resonances become increasingly apparent at higher frequencies (> 1.1 GHz), while the number of cladding-confined acoustic modes involved in scattering falls. Two main types of scattering are observed: intramodal (scattering to new frequencies within the same optical mode) and intermodal (frequency-shifted scattering to a different optical mode). It is shown that the twofold symmetric microstructure in a birefringent fiber causes strongly polarization-dependent intramodal scattering. Good agreement is obtained between the experimental measurements and numerical solutions of both the acoustic and electromagnetic wave equations by using a full-vectorial finite-element approach. Phononic bandgaps are found to play a significant role at higher air-filling fractions, leading to the appearance of additional bands in the scattering spectrum. (C) 2009 Optical Society of America

Journal of the Optical Society of America B-Optical Physics 26[8], 1641-1648. 2009.

P182-09 "Influence of chemical interesterification on thermal behavior, microstructure, polymorphism and crystallization properties of canola oil and fully hydrogenated cottonseed oil blends"

Ribeiro, A. P. B., Basso, R. C., Grimaldi, R., Gioielli, L. A., dos Santos, A. O., Cardoso, L. P., and Goncalves, L. A. G.

This work evaluated chemical interesterification of canola oil (CaO) and fully hydrogenated cottonseed oil (FHCSO) blends, with 20%, 25%, 30%, 35% and 40%(w/w) FHCSO content. Interesterification produced reduction of trisaturated and increase in monounsaturated and diunsaturated triacylglycerols contents, which caused important changes in temperatures and enthalpies associated with the crystallization and melting thermograms. It was verified reduction in medium crystal diameter in all blends, in addition crystal morphology modification. Crystallization kinetics revealed that crystal formation induction period and maximum solid fat content were altered according to FHCSO content in original blends and as a result of random rearrangement. Changes in Avrami constant (k) and exponent (n) indicated, respectively, that interesterification decreased crystallization rates and altered crystalline morphology. However, X-ray diffraction analyses showed randomization did not change the original crystalline polymorphism. The original and interesterified blends had significant predominance of beta' polymorph, which is interesting for several food applications. (C) 2009 Elsevier Ltd. All rights reserved

Food Research International 42[8], 1153-1162. 2009.

P183-09 "Influence of propagation on the coherent accumulation of excitation induced by an ultrashort pulse train"

Soares, A. A. and de Araujo, L. E. E.

We study the effects of propagation through an extended sample of two- and three-level atoms on the coherent accumulation of excitation by an ultrashort pulse train. In the two- level case, previous pulses in the train may prepare the medium such that a later pulse may experience amplification and absorption in different positions inside the sample. For a large number of pulses, the atomic medium may be saturated by the train, and some pulses propagate without experiencing either absorption or amplification. In general, absorption of the resonant pulse frequency during propagation compromises the accumulation efficiency. In the three-level case, the coherent accumulation of excitation leads to electromagnetically induced transparency of the pulse train, and the pulses exit the medium without any distortion in their temporal profile

Physical Review A 80[1], 013832. 2009.

P184-09 "K/pi Fluctuations at Relativistic Energies"

Abelev, B. I., Aggarwal, M. M., Ahammed, Z., Anderson, B. D., Arkhipkin, D., Averichev, G. S., Balewski, J., Barannikova, O., Barnby, L. S., et all

We report K/pi fluctuations from Au+Au collisions at s(NN)=19.6, 62.4, 130, and 200 GeV using the STAR detector at the Relativistic Heavy Ion Collider. K/pi fluctuations in central collisions show little dependence on incident energy and are on the same order as those from NA49 at the Super Proton Synchrotron in central Pb+Pb collisions at s(NN)=12.3 and 17.3 GeV. We report results for the collision centrality dependence of K/pi fluctuations and results for charge-separated fluctuations. We observe that the K/pi fluctuations scale with the charged particle multiplicity density

Physical Review Letters 103[9], 092301. 2009.

P185-09 "Likelihood for supernova neutrino analyses"

Ianni, A., Pagliaroli, G., Strumia, A., Torres, F. R., Villante, F. L., and Vissani, F.

We derive the event-by-event likelihood that allows us to extract the complete information contained in the energy, time, and direction of supernova neutrinos, and specify it in the case of SN1987A data. We resolve discrepancies in the previous literature, numerically relevant already in the concrete case of SN1987A data

Physical Review D 80[4] ,043007. 2009.

P186-09 "Measuring Red Blood Cells Electrical Membrane Charges Using Optical Tweezers"

Fernades, H. P., Fontes, A., de Thomaz, A. A., Barbosa, L., Silva, D. N., Castro, V., Barjas-Castro, M. L., and Cesar, C. L.

Transfusion 49, 138A. 2009.

P187-09 "Microstrip resonators for electron paramagnetic resonance experiments"

Torrezan, A. C., Alegre, T. P. M., and Medeiros-Ribeiro, G.

In this article we evaluate the performance of an electron paramagnetic resonance (EPR) setup using a microstrip resonator (MR). The design and characterization of the resonator are described and parameters of importance to EPR and spin manipulation are examined, including cavity quality factor, filling factor, and microwave magnetic field in the sample region. Simulated microwave electric and magnetic field distributions in the resonator are also presented and

compared with qualitative measurements of the field distribution obtained by a perturbation technique. Based on EPR experiments carried out with a standard marker at room temperature and a MR resonating at 8.17 GHz, the minimum detectable number of spins was found to be 5x10(10) spins/GHz(1/2) despite the low MR unloaded quality factor Q(0)=60. The functionality of the EPR setup was further evaluated at low temperature, where the spin resonance of Cr dopants present in a GaAs wafer was detected at 2.3 K. The design and characterization of a more versatile MR targeting an improved EPR sensitivity and featuring an integrated biasing circuit for the study of samples that require an electrical contact are also discussed

Review of Scientific Instruments 80[7], 075111. 2009.

P188-09 "Monogamy inequality and residual entanglement of three qubits under decoherence"

de Oliveira, T. R.

Exploring an analytical expression for the convex roof of the pure state squared concurrence for rank 2 mixed states the entanglement of a system of three particles under decoherence is studied, using the monogamy inequality for mixed states and the residual entanglement obtained from it. The monogamy inequality is investigated both for the concurrence and the negativity in the case of local independent phase damping channel acting on generalized Greenberger-Horne-Zeilinger states of three particles and the local independent amplitude damping channel acting on generalized |W >=|001 >+|010 >+|100 > state of three particles. It is shown that the bipartite entanglement between one qubit and the rest has a qualitative similar behavior to the entanglement between individual qubits, and that the residual entanglement in terms of the negativity cannot be a good entanglement measure for mixed states, since it can increase under local decoherence

Physical Review A 80[2], 022331. 2009.

P189-09 "Multiple scattering x-ray photoelectron diffraction study of the SrTiO3(100) surface"

Pancotti, A., Barrett, N., Zagonel, L. F., and Vanacore, G. M.

The atomic surface structure of SrTiO3(100) after annealing at 630 degrees C in vacuum is investigated by x-ray photoelectron diffraction (XPD) using the Sr 3d(5/2) core level. The photoelectron diffraction peaks are successfully assigned by considering the forward scattering of photoelectrons by the atomic potential near the emitter atom in the lattice. The strongest diffraction peaks are aligned along the single crystal internuclear axes. We compare the results of photoelectron multiple scattering calculations (MSC) of SrO and TiO2 terminated SrTiO3(100) surfaces, including surface relaxation and rumpling, with the experimental data. For TiO2 and SrO terminated SrTiO3(100) surfaces, all top-layer cations relax inward, whereas second-layer atoms relax outward. The surface rumpling for SrO- and TiO2-terminated surfaces agrees well with low-energy electron diffraction results. Using a genetic algorithm the best agreement of MSC to the experimental XPD data is obtained for a SrO terminated surface with a 30% coverage of 3 ML SrO(100) islands

Journal of Applied Physics 106[3], 034104. 2009.

P190-09 "On the determination of the magnetic entropy change in materials with first-order transitions"

Caron, L., Ou, Z. Q., Nguyen, T. T., Thanh, D. T. C., Tegus, O., and Bruck, E.

An accurate method to determine the magnetic entropy change in materials with hysteretic first-order transitions is presented, which is needed to estimate their potential for applications. We have investigated the effect of the maximal entropy change derived from magnetization measurements performed in different measurement processes. The results show that the isothermal entropy change can be derived from the Maxwell relations even for samples with large thermal hysteresis. In the temperature region with hysteresis, over estimating the entropy change can be avoided by measuring the isothermal magnetization of the sample after it is cooled from the paramagnetic state to the measurement temperature. In this way the so-called peak effect is not observed as shown here for a few compounds. (C) 2009 Elsevier B.V. All rights reserved

Journal of Magnetism and Magnetic Materials 321[21], 3559-3566. 2009.

P191-09 "On the origins of the scalar and vectorial product definitions"

Menon, M. J.

The operations of two vector multiplication (the scalar and vector products) are introduced in physics and mathematics textbooks just as a definition, without any reference or discussion oil the formal reasons and/or motivations that have led to these structures. In this work, a short pedagogical review on the origins of these definitions is presented. We discuss the formal results obtained by Hamilton in the context of quaternionic algebra and some "changes" performed by Gibbs and Heaviside, leading to what is now usually known as "vector algebra". We present comments on some disadvantages of these "changes", referring to more practical and formal systems (Grassmann and Clifford algebras). Some basic and recent works on the subject are also mentioned and commented

Revista Brasileira de Ensino de Fisica 31[2], 2305. 2009.

P192-09 "Pion interferometry in Au plus Au and Cu plus Cu collisions at s(NN)=62.4 and 200 GeV"

Abelev, B. I., Aggarwal, M. M., Ahammed, Z., Anderson, B. D., Arkhipkin, D., Averichev, G. S., Balewski, J., Barannikova, O., Barnby, L. S., et all

We present a systematic analysis of two-pion interferometry in Au+Au collisions at s(NN)=62.4 GeV and Cu+Cu collisions at s(NN)=62.4 and 200 GeV using the STAR detector at the Relativistic Heavy Ion Collider (RHIC). The multiplicity and transverse momentum dependences of the extracted correlation lengths (radii) are studied. The scaling with charged particle multiplicity of the apparent system volume at final interaction is studied for the RHIC energy domain. The multiplicity scaling of the measured correlation radii is found to be independent of colliding system and collision energy

Physical Review C 80[2], 024905. 2009.

P193-09 "Pressure induced magnetic and magnetocaloric properties in NiCoMnSb Heusler alloy"

Nayak, A. K., Suresh, K. G., Nigam, A. K., Coelho, A. A., and Gama, S.

The effect of pressure on the magnetic and the magnetocaloric (MC) properties around the martensitic transformation temperature in NiCoMnSb Heusler alloy has been studied. The martensitic transition temperature has significantly shifted to higher temperatures with pressure, whereas the trend is opposite with the application of applied magnetic field. The maximum magnetic entropy change around the martensitic transition temperature for Ni45Co5Mn38Sb12 is 41.4 J/kg K at the ambient pressure, whereas it is 33 J/kg K at 8.5 kbar. We find that by adjusting the Co concentration and applying suitable pressure, NiCoMnSb system can be tuned to achieve giant MC effect spread over a large temperature span around the room temperature, thereby making it a potential magnetic refrigerant material for applications

Journal of Applied Physics 106[5], 053901. 2009.

P194-09 "Robustness of quantum discord to sudden death"

Werlang, T., Souza, S., Fanchini, F. F., and Boas, C. J. V.

We calculate the dissipative dynamics of two-qubit quantum discord under Markovian environments. We analyze various dissipative channels such as dephasing, depolarizing, and generalized amplitude damping, assuming independent perturbation, in which each qubit is coupled to its own channel. Choosing initial conditions that manifest the so-called sudden death of entanglement, we compare the dynamics of entanglement with that of quantum discord. We show that in all cases where entanglement suddenly disappears, quantum discord vanishes only in the asymptotic limit, behaving similarly to individual decoherence of the qubits, even at finite temperatures. Hence, quantum discord is more robust than the entanglement against decoherence so that quantum algorithms based only on quantum discord correlations may be more robust than those based on entanglement

Physical Review A 80[2], 024103. 2009.

P195-09 "Searching for the Fractional Quantum Hall Effect in Graphite"

Kopelevich, Y., Raquet, B., Goiran, M., Escoffier, W., da Silva, R. R., Pantoja, J. C. M., Luk'yanchuk, I. A., Sinchenko, A., and Monceau, P.

Measurements of basal plane longitudinal rho(b)(B) and Hall rho(H)(dB) resistivities were performed on highly oriented pyrolytic graphite samples in a pulsed magnetic field up to B = 50 T applied perpendicular to graphene planes, and temperatures 1.5 K <= T <= 4.2 K. At B > 30 T and for all studied samples, we observed a sign change in rho(H)(B) from electron- to holelike. For our best quality sample, the measurements revealed the enhancement in rho(b)(B) for B > 34 T (T = 1.8 K), presumably associated with the field-driven charge density wave or Wigner crystallization transition. In addition, well-defined plateaus in rho(H)(B) were detected in the ultraquantum limit revealing possible signatures of the fractional quantum Hall effect in graphite

Physical Review Letters 103[11], 116802. 2009.

P196-09 "Simultaneous observation of the magnetic and electric behavior in a correlated system near a metal-semiconductor transition: ESR in pellets of conducting polymers"

Kondo, J. M., Walmsley, L., Rettori, C., Sercheli, M. S., Correa, A. A., and Pereira, E. C.

Electron spin resonance (ESR) experiments show, at the metal-semiconductor transition temperature of a conducting polymer, the distinct contributions of the disordered and crystalline regions. In the more disordered regions of the polymer the polarons experience an antiferromagnetic coupling. As the level of disorder decreases, when small crystalline regions appear, there is a tendency, in some temperature range, for the polarons to interact ferromagnetically. For more ordered regions or crystalline regions of larger sizes, there is a competition between localized ferromagnetic coupled polarons and delocalized ones, that is, between localization and delocalization. The possibility to fit the ESR data for one of the samples using two Dysonian lines, one for each phase, allows one to follow the general behavior of the microwave conductivity as a function of the temperature. The semiconducting behavior of the disordered phase is clearly observed, as well as the true metallic behavior of the crystalline phase revealed by the increase in conductivity with the decrease in temperature

Physical Review B 80[1], 014410. 2009.

P197-09 "Single-Wall Carbon Nanotubes Chemically Modified with Cysteamine and Their Application in Polymer Solar Cells: Influence of the Chemical Modification on Device Performance"

Conturbia, G., Vinhas, R. D. G., Landers, R., Valente, G. M. S., Baranauskas, V., and Nogueira, A. F.

In order to improve the dispersion of single-wall carbon nanotubes in a matrix of poly(3-hexylthiophene), this paper reports the modification of single-wall carbon nanotubes with COOH groups followed by reaction with cysteamine that introduced thiol groups along the tubes. The resulting modified single-wall carbon nanotubes were characterized by high resolution transmission electron microscopy, thermogravimetric analysis, X-ray photoelectron spectroscopy and Raman spectroscopy. The modified carbon nanotubes were applied, in combination with poly(3-hexylthiophene), in a bulk heterojunction solar cell. After passing through a post-treatment process to obtain debundled modified single-wall carbon nanotubes, solar cells with improved performance were obtained. After the treatment sequence, both the open circuit voltage and short-circuit current increased in comparison to the non-treated modified single-wall carbon nanotubes polymer solar cells

Journal of Nanoscience and Nanotechnology 9[10], 5850-5859. 2009.

P198-09 "Spin density wave dislocation in chromium probed by coherent X-ray diffraction"

Jacques, V. L. R., Le Bolloc'h, D., Ravy, S., Giles, C., Livet, F., and Wilkins, S. B.

We report on the study of a magnetic dislocation in pure chromium. Coherent X-ray diffraction profiles obtained on the incommensurate Spin Density Wave (SDW) reflection are consistent with the presence of a dislocation of the magnetic

order, embedded at a few micrometers from the surface of the sample. Beyond the specific case of magnetic dislocations in chromium, this work may open up a new method for the study of magnetic defects embedded in the bulk

European Physical Journal B 70[3], 317-325. 2009.

P199-09 "Synchrotron x-ray multiple diffraction in the study of Fe+ ion implantation in Si(001)"

dos Santos, A. O., Lang, R., de Menezes, A. S., Meneses, E. A., Amaral, L., Reboh, S., and Cardoso, L. P.

In this work, x-ray multiple diffraction has been used as a three-dimensional high-resolution probe to study the Fe+ ion implantation process in Si(0 0 1). The semiconducting beta-FeSi2 crystallographic phase has been synthesized by Fe ion co-implantation in Si(0 0 1) followed by ion-beam-induced epitaxial crystallization (IBIEC) and thermal treatment. This phase was clearly detected by the conventional techniques, micro-Raman scattering spectroscopy, transmission electron microscopy (TEM) and grazing incidence x-ray diffraction. Synchrotron radiation rocking curves (omega-scans) and mapping of the Bragg surface diffraction (BSD) of the Si matrix, as-implanted, after the IBIEC process and thermally treated, have enabled the detection of co-implanted regions formation that present distinct lattices in comparison with the matrix one clearly observed by TEM. Also, the compressive strain of both regions in depth by rocking curve and in-plane has been determined by using BSD, which is one order of magnitude smaller

Journal of Physics D-Applied Physics 42[19], 195401. 2009.

P200-09 "The structure and dynamics of boron nitride nanoscrolls"

Perim, E. and Galvao, D. S.

Carbon nanoscrolls (CNSs) are structures formed by rolling up graphene layers into a scroll-like shape. CNNs have been experimentally produced by different groups. Boron nitride nanoscrolls (BNNSs) are similar structures using boron nitride instead of graphene layers. In this paper we report molecular mechanics and molecular dynamics results for the structural and dynamical aspects of BNNS formation. Similarly to CNS, BNNS formation is dominated by two major energy contributions, the increase in the elastic energy and the energetic gain due to van der Waals interactions of the overlapping surface of the rolled layers. The armchair scrolls are the most stable configuration while zigzag scrolls are metastable structures which can be thermally converted to armchairs. Chiral scrolls are unstable and tend to evolve into zigzag or armchair configurations depending on their initial geometries. The possible experimental routes to produce BNNSs are also addressed

Nanotechnology 20[33], 335702. 2009.

P201-09 "Theoretical investigation of electron collisions with sulfur monoxide in the low- and intermediate-energy range"

Lee, M. T., Iga, I., Machado, L. E., and Brescansin, L. M.

We report a theoretical study on electron collisions with the sulfur monoxide radical. More specifically, differential, integral, and momentum-transfer cross sections are calculated and reported in the 1-500 eV energy range. Calculations are performed at the static-exchange-polarization-absorption level of approximation. A combination of the iterative Schwinger variational method and the distorted-wave approximation is used to solve the scattering equations. Our study reveals shape resonances in both the doublet and quartet spin-specific scattering channels. The occurrence of such resonances may enhance the spin-flip effects. In addition, the comparison of our calculated total absorption cross sections with existing experimental total ionization cross sections is encouraging

Physical Review A 80[2], 022706. 2009.

P202-09 "Upper limit on the cosmic-ray photon fraction at EeV energies from the Pierre Auger Observatory"

Abraham, J., Abreu, P., Aglietta, M., Aguirre, C., Ahn, E. J., Allard, D., Allekotte, I., Allen, J., Allison, P., varez-Muniz, J., Ambrosio, M., Anchordoqui, L., Andringa, S., Anzalone, A., Aramo, C., et all

From direct observations of the longitudinal development of ultra-high energy air showers performed with the Pierre Auger Observatory, upper limits of 3.8%, 2.4%, 3.5% and 11.7% (at 95% c.l.) are obtained on the fraction of cosmic-ray photons above 2, 3, 5 and 10 EeV (1 EeV equivalent to 10(18) eV), respectively. These are the first experimental limits on ultra-high energy photons at energies below 10 EeV. The results complement previous constraints on top-down models from array data and they reduce systematic uncertainties in the interpretation of shower data in terms of primary flux, nuclear composition and proton-air cross-section. (C) 2009 Elsevier B.V. All rights reserved

Astroparticle Physics 31[6], 399-406. 2009.

P203-09 "Valence-bond theory of highly disordered quantum antiferromagnets"

Zhou, S., Hoyos, J. A., Dobrosavljevic, V., and Miranda, E.

We present a large-N variational approach to describe the magnetism of insulating doped semiconductors based on a disorder-generalization of the resonating-valence-bond theory for quantum antiferromagnets. This method captures all the qualitative and even quantitative predictions of the strong-disorder renormalization group approach over the entire experimentally relevant temperature range. Finally, by mapping the problem on a hard-sphere fluid, we could provide an essentially exact analytic solution without any adjustable parameters. Copyright (C) EPLA, 2009

Epl 87[2], 27003. 2009.

Abstracta

Instituto de Física
Diretor: Prof. Dr. Julio Cesar Hadler Neto
Universidade Estadual de Campinas - UNICAMP
Cidade Universitária C.P. 6165
CEP: 13081-970 - Campinas - SP - Brasil
e-mail: secdir@ifi.unicamp.br
Fone: 0XX 19 3521-5300

Publicação

Biblioteca do Instituto de Física Gleb Wataghin
http://webbif.ifi.unicamp.br
Diretora Técnica: Sandra Maria Carlos Cartaxo

Elaboração
Antonela Carvalho Ribeiro
antonela@ifi.unicamp.br

Projeto Gráfico
ÍgneaDesign

Impressão
Gráfica Central - Unicamp